J Therm Anal Calorim (2016) 126:1447–1453
DOI 10.1007/s10973-016-5735-9

Structural and thermodynamic properties of nanocrystalline Cr_3C_2–25(Ni20Cr) composite powders produced by high-energy ball milling

Cecílio A. Cunha[1] · Olandir V. Correa[1] · Issac J. Sayeg[2] · Nelson B. Lima[1] · Lalgudi V. Ramanathan[1]

Received: 9 October 2015 / Accepted: 19 July 2016 / Published online: 26 July 2016

Abstract Nanostructured coatings have been used to protect components exposed to severe service conditions. High energy milling is widely used to produce nanocrystalline feedstock of coating materials such as chromium carbide and tungsten carbide. This paper presents the structural and thermodynamic properties of Cr_3C_2–25(Ni20Cr) powders that were high energy milled for different times. During the high energy milling of Cr_3C_2–25(Ni20Cr) powder, severe plastic deformation takes place. A small part of the energy spent in this process is stored in the crystal lattice as deformation energy. The crystallite size and microstrain in nanocrystalline Cr_3C_2–25(Ni20Cr) powders milled for different times were determined by X-ray diffraction measurements. Differential scanning calorimetric (DSC) studies of the milled powders revealed a broad transformation, characteristic of a large exothermic reaction in the nanostructured powder. The enthalpy variation measured by DSC permitted determination of the deformation energy stored in the Cr_3C_2–25(Ni20Cr) powders milled for different times. These measurements also enabled calculation of the specific heat variation of the milled powders.

Keywords Cr_3C_2–25(Ni20Cr) · Crystallite size · Microstrain · Thermodynamic properties

Introduction

The pioneering work of Benjamin [1], Benjamin and Volin [2], and Gilman and Benjamin [3] that established the process which became globally known as "Mechanical Alloying", has been considerably improved during the last three decades. In this process, carried out by high energy milling, extensive cold work produces a high degree of microstructural refinement and this results in nanocrystalline or non-equilibrium structures [4–7]. In recent years, interest in coatings prepared with nanostructured materials has increased significantly, as these coatings exhibit higher hardness and strength compared with those coatings prepared with conventional materials [1–15]. The improved properties of nanostructured materials are related to the very small grain (or crystallite) size and to the high volume fraction of grain boundaries and interfaces [5, 7, 16, 17]. It is widely accepted that in materials with very small crystallite size ($\leq$30 nm), a large proportion of the atoms are at grain and/or interface boundaries compared to those within the grain [5, 16–20]. Several methods have been used to synthesize nanostructured materials, and these include cryogenic processes as well [4–11, 19–30]. Chromium carbide or other carbide-based powders for use as feedstock to produce nanostructured coatings are often prepared by high energy milling [4–7, 9–11, 20–27].[1] Many chromium carbide-based coatings are in use, and these usually contain

✉ Lalgudi V. Ramanathan
lalgudi@ipen.br

[1] Instituto de Pesquisas Energéticas e Nucleares, IPEN-CNEN-SP, Av. Prof. Lineu Prestes 2242, Cidade Universitária, São Paulo 05508-000, Brazil

[2] Instituto de Geociências da Universidade de São Paulo – USP, Rua do Lago 562, Cidade Universitária, São Paulo 05508-080, Brazil

[1] Powders of Cr_3C_2–25(Ni20Cr) produced in this investigation were used to prepare HVOF-sprayed nanostructured coatings, and these were tested in a custom-designed high temperature erosion–oxidation rig. The results were presented in "Mechanical properties and erosion–oxidation resistance of thermally sprayed nanostructured Cr_3C_2–25(Ni20Cr) coatings" at the 26th International Surface Modification Technologies, 2012, Lyon, France.

a metallic binder phase like NiCr, with Cr in the range of 10–30 %.

This paper presents the structural and thermodynamic properties of nanocrystalline Cr_3C_2–25(Ni20Cr) powders prepared by high-energy ball milling for different times. It is well known that when metals are submitted to severe plastic deformation, as in high-energy ball milling, most of the mechanical energy is converted into heat, but a small portion of the energy is retained in the crystal lattice as "deformation energy" [31]. Cotteril and Mould [32] reported that the retained energy represents the energy of disorder produced by deformation ("the driving force for recovery and recrystallization processes"). In high energy milled Cr_3C_2–25(Ni20Cr) powder, the deformation energy is stored mainly in the Ni20Cr solid solution, and it can be determined from enthalpy variation of the powder milled for different times. Taking into account that the microstrain introduced in the crystalline structure by the high-energy milling process contributes to lattice deformation, determination of the "deformation energy" stored in the crystal lattice, that is, the enthalpy variation, also permits calculation of specific heat variation of the Ni20Cr solid solution as a function of milling time.

Methods and materials

A high-energy ball-milling device (ZOZ) was used to mill Cr_3C_2–25(Ni20Cr) powders. The stainless steel vessel of this mill had an approximate volume of 2000 cm^3. Chromium steel balls 4.7 mm in diameter were used with gaseous nitrogen as the milling medium. The main powder milling parameters were 400 rpm, ball-to-powder ratio 10:1 (1 kg of steel balls were used for 100 g of powder to be milled) and milling times 2, 4, 8, 16, 20, 24, 32 and 64 h. Further details about powder preparation and powder characteristics can be found elsewhere [9–11].

The crystallite size of the milled powders as well as the microstrain at the atomic level in the crystal lattice was determined by X-ray diffraction analyses [33–36]. This was carried out using the Rietveld method for lattice refinement [37–40]. The mean crystallite size as a function of milling time, as well as the microstrain (%) in the crystal lattice as a function of the crystallite size, was determined using the "Linear Fitting" approach, the details of which can be found in other studies [5, 33–36]. A transmission electron microscope, model JEM-2100, was used to study the microstructure of the binder phase in the milled powders and to evaluate the crystallite size. The latter was done to compare with that determined by X-ray diffraction analysis. Differential scanning calorimetric (DSC) measurements of powders milled for different times were taken with a DSC-50 (Shimadzu) equipment, in which ~40 mg samples and a flux of pure argon at 30 l min^{-1} were used. The heating rate was 10 °C min^{-1}, and the temperature range 22–500 °C. To maintain consistency, the different parameters were plotted as a function of the reciprocal of crystallite size, based on the suggestion of Hellstern et al. [20]. They supported this approach on the basis that the ratio of atoms close to grain boundaries to those within the crystal is proportional to $1/D$. Further, they observed that milling time provides only an arbitrary scale for evaluation of material properties, because milling time depends on process parameters, such as type, material and size of the vessel, size and material of the balls, ball-to-powder ratio.

Results and discussion

Crystallite size and microstrain

The X-ray diffractograms of the "as-received" powders, and the powders milled for different times are shown in Fig. 1. Evidence of structural changes in the milled powders can be observed from broadening of the X-ray diffraction peaks.

The mean crystallite size of the Cr_3C_2–25(Ni20Cr) powders as a function of milling time and the microstrain (%) at the atomic level produced in the crystal lattice by severe plastic deformation are shown in Fig. 2a, b. These two parameters, crystallite size and microstrain were determined using the linear fitting approach [5, 33–36], represented by Eq. (1),

$$\Delta(2\theta)\cos\theta = 2\varepsilon\sin\theta + 0.9\lambda/D \quad (1)$$

where D is the crystallite size, ε is the microstrain, λ is the wavelength (Cu target, $\lambda = 1.54$ A), $\Delta(2\theta)$ is the full width at half maximum (FWHM), and θ is the diffraction angle.

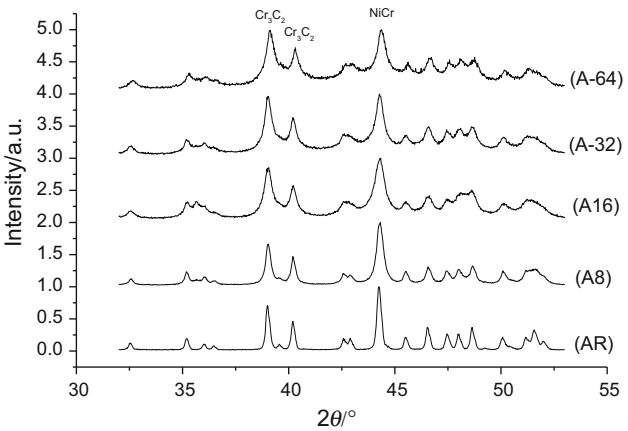

Fig. 1 X-ray diffractograms of Cr_3C_2–25(Ni20Cr) powders in the "as-received" condition and after milling for different times

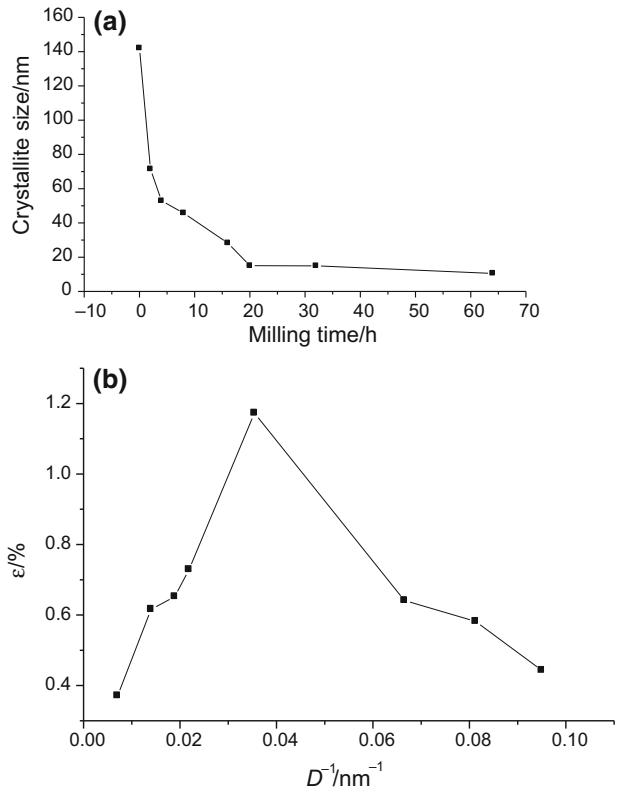

Fig. 2 **a** Mean crystallite size and **b** microstrain (%) of the nanostructured Cr_3C_2–25(Ni20Cr) powders

Five peaks ($2\theta = 44.2$; 51.5; 75.9; 92.4; 97.8) corresponding to the NiCr alloy in the spectrums were used to calculate the full width at half maximum (FWHM).

Figure 2a shows that as milling time increased the crystallite size decreased [5–7, 9–11, 20–26]. This figure also shows that in the initial stages of ball milling, crystallite size decreased rapidly to <50 nm and further decrease in crystallite size to ~10 nm occurred slowly. Transmission electron microscopy enabled direct observation of the crystallite size and other microstructural features in the nanostructured powders. Figure 3a, b shows bright field transmission electron micrographs of nanostructured powders milled for 8 and 64 h, respectively. The mean crystallite sizes observed by TEM were in good agreement with those determined by X-ray diffraction analyses. Figure 3c shows two edge dislocations in the microstructure of the matrix phase of Cr_3C_2–25(Ni20Cr) powder milled for 64 h, as well as the distortion produced in the crystal lattice close to these dislocations.

As shown in Fig. 2b, deformation of the crystal lattice during the milling process causes an increase in microstrain at the atomic level with a maximum of 1.17 % in samples which had mean crystallite size of 28 nm—that is, in powder milled for 16 h. As reported in other studies [5, 20], formation of a nanocrystalline structure is considered to originate from development of dislocation cell structures inside shear bands. According to this mechanism, referred to as "dislocation cell evolution," they affirmed that during mechanical milling, the powder particles are continuously deformed by impact loads, the direction of which changes randomly during the milling process. This random cyclic loading and consequent deformation of the crystalline lattice suggests establishment of a strain fatigue process or a low cycle fatigue process [5, 20]. However, the work of Plumtree and Pawlus [41], who worked with aluminum samples, reported that the primary characteristic of the deformed microstructure caused by a conventional strain fatigue process is due to development of dislocation cells. They however did not observe grain refinement, and accordingly, their results suggest that the development of dislocation cells during the conventional fatigue process does not promote refinement of the microstructure. However, as mentioned elsewhere [5, 20], there are probably significant differences in loading characteristics (amplitude and number of cycles) between conventional strain fatigue processes and high energy milling. On the basis of this, it is reasonable to state that the central hypothesis is still valid. That is, a possible correlation exists between the dislocation cell mechanism and the formation of nanocrystalline structure during high energy milling.

The increase in microstrain to a maximum, followed by its decrease with further reduction in crystallite size beyond 28 nm indicates existence of a critical crystallite size, which could be represented as follow:

$$\partial\varepsilon/\partial(1/D) = 0 \Rightarrow \varepsilon_{\max} = 1.17\ \% \quad \text{and}$$
$$D = D_{\mathrm{CRIT}} = 28\ \mathrm{nm}$$

The microstrain at the atomic level is related to dislocation density in the material and stability of the dislocation structure. As the material approaches the critical crystallite size, the dislocation structure in it becomes unstable, favoring its dissociation into partial dislocations (Shockley partials), which are known to be more stable than the dislocations from which they originated. Consequently, there is a reduction in the strain energy, and this in turn reduces the microstrain (%) at the atomic level.

$$\rho_{\mathrm{dislocations}}(\varepsilon_{\max}) \Rightarrow \text{Dissociation of dislocations: } a/2(110) \rightarrow {}^{a/6(211)}_{a/6(12\bar{1})} + \cdots$$
$$\Rightarrow \downarrow E_{\mathrm{def}} \Rightarrow \downarrow \varepsilon(\%)$$

At grain sizes of the order of the critical crystallite size (28 nm in this investigation) a large number of the atoms present in the material are at grain boundaries [5, 16, 19, 20, 42, 43]. It is well known that in the final stages of deformation, the dislocations migrate to the grain boundary leaving the interior of the grains almost free of

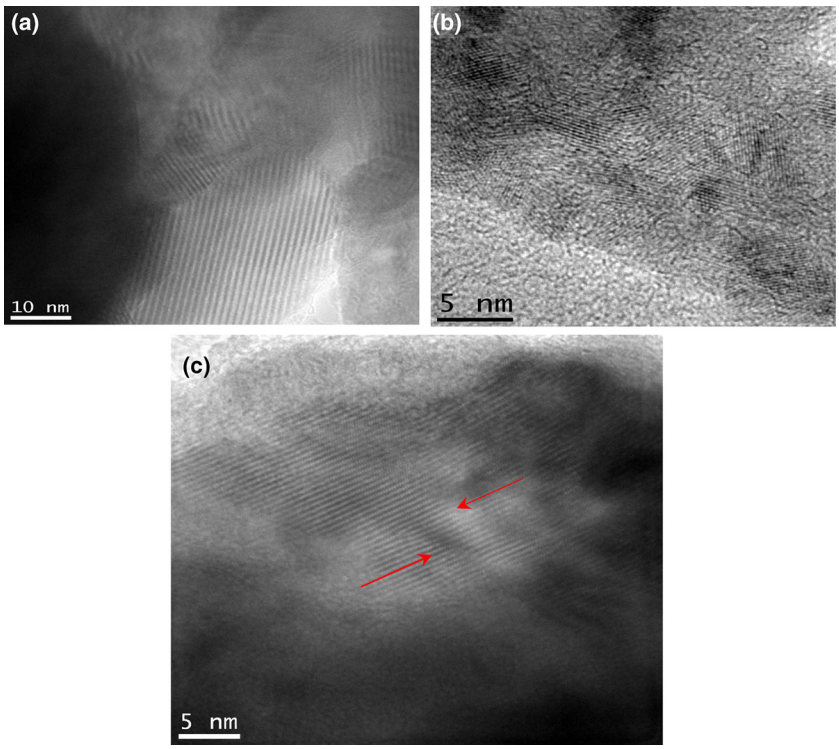

Fig. 3 TEM bright field image showing: **a** nanosized grains in Cr_3C_2–*25*(Ni20Cr) powder milled for 8 h; **b** nanosized grains in Cr_3C_2–*25*(Ni20Cr) powder milled for 64 h; **c** dislocations in the microstructure of Cr_3C_2–*25*(Ni20Cr) powder milled for 64 h—the *arrows* indicate two edge dislocations of different signs, i.e., had these dislocations been in the same slip plane they would annihilate one another under the action of an external force. *Note* the distortion produced in the crystal lattice close to these dislocations

dislocations. On the basis of observations made by Wolf et al. [44], our results suggest that after attaining the critical crystallite size, the influence of the grain boundaries becomes more significant in the deformation process than the mechanism of slipping dislocations. This phenomenon is usually mentioned as the inverted Hall–Petch effect. The change in the behavior of the Hall–Petch effect for a specific critical crystallite size, typically in the range of 20–30 nm, observed in some experiments, is considered to be related to change in the dominant deformation mechanism, i.e., from a mechanism based on dislocation processes to a mechanism controlled by processes existent at the grain boundaries ("grain boundary sliding"). Under these circumstances, i.e., when the material's crystallite size nears the critical value, the activity of the dislocations inside the grains starts to cease due to the reduced crystallite size. This fact is not only related to the occurrence of the inverted Hall–Petch effect, but it also permits explanation of this effect (i.e., under these conditions, the "dislocation pile-up" effect almost seizes) [45].

Enthalpy and specific heat variation

As for the energy stored in the crystal lattice, DSC analyses of the nanostructured powders revealed a broad transformation in the temperature range ~120 to ~450 °C, indicating that a large exothermic reaction occurred in the powders. The DSC analysis curves of the powders milled for 2, 4, 8, 16, 20, 24, 32 and 64 h were quite similar, and Fig. 4 shows the curve for the powder milled for 16 h.

Data extracted from the different DSC curves were used to plot enthalpy variation and energy peak height as a function of the reciprocal of crystallite size (which is related to milling time). These plots are shown in Fig. 5a, b. These figures clearly show that enthalpy variation indeed reached a maximum in powders milled for 16 h, and the heat released from the exothermic reaction was of the order of 3025 mJ. Similar observations were made with regard to the energy peak height of the powders milled for 16 h, which reached a maximum value of 2.78 mW. The explanation for decrease in these two parameters with increase in milling time beyond 16 h is the same as that suggested above to explain the reduction in microstrain at the atomic level. That is, with reduction in strain energy, there is a reduction in "deformation energy" stored in the crystal lattice, which causes reduction in enthalpy variation and energy peak height.

Regarding calculation of specific heat variation, it is worth mentioning that when pressure is constant (basic

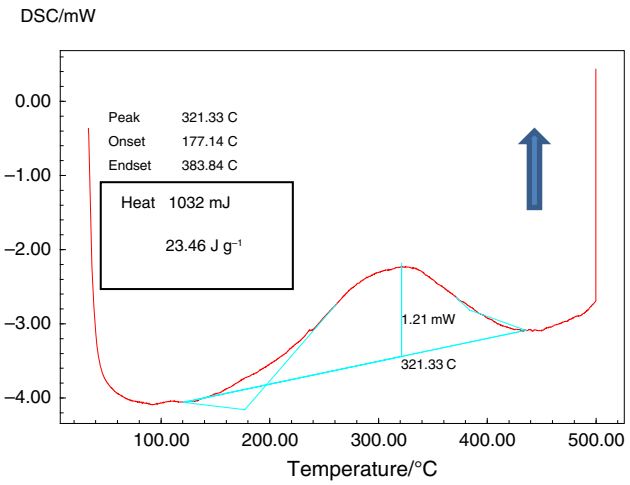

Fig. 4 DSC analysis of Cr_3C_2–25(Ni20Cr) powder milled for 16 h. *Note* the broad transformation in the temperature range ~120 to ~450 °C, indicating a large exothermic reaction in the powder

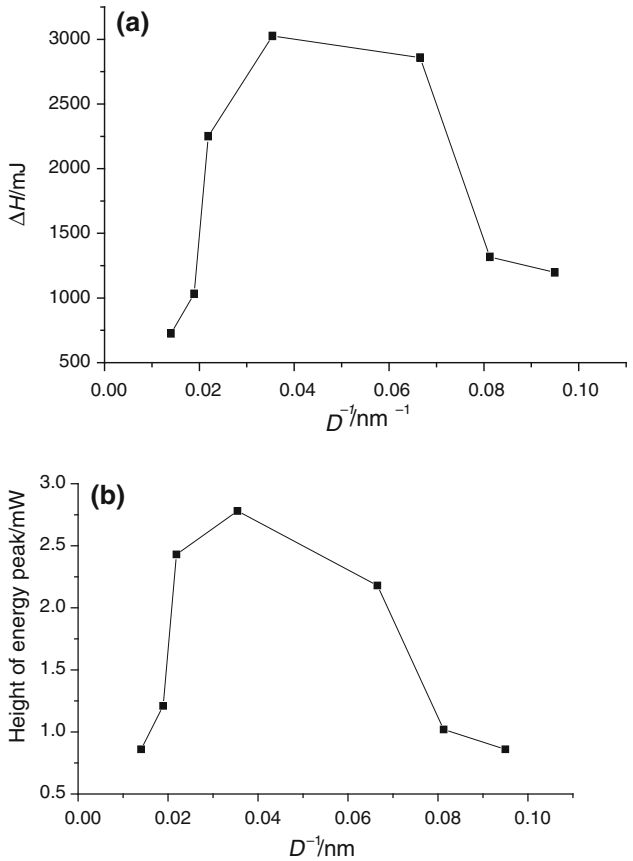

Fig. 5 **a** Enthalpy variation as a function of reciprocal of crystallite size. *Note* that the maximum heat release occurred in powders milled for 16 h. **b** Variation of energy peak height as a function of reciprocal of crystallite size. The maximum in this case also occurred in powders milled for 16 h

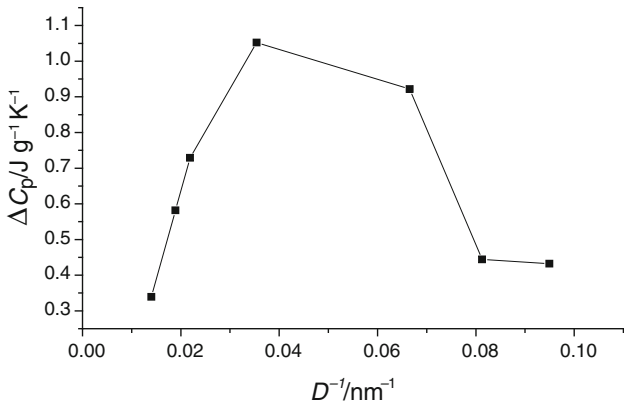

Fig. 6 Specific heat variation as a function of the reciprocal of crystallite size. *Note* that the maximum variation occurred in powder with mean crystallite size of 28 nm (i.e., powder milled for 16 h)

condition for tests performed in DSC equipment [46]) $dQ = d(\Delta H)$. This permits determination of the variation in specific heat of the material, which is related to plastic deformation introduced in the crystal lattice. The well-known Eq. (2) relates heat given off or absorbed during a reaction and the specific heat.

$$Q = m\,C_p \Delta T \tag{2}$$

This can be rewritten as

$$\Delta C_p = (\Delta H)/m\,\Delta T \tag{3}$$

Since the values on the right side of Eq. (3) are known for the different powder milling conditions, the specific heat variation of powders milled for different times could be calculated. The specific heat variation as a function of the reciprocal of crystallite size is shown in Fig. 6. Once again, it can be noted that the maximum variation occurred for powder with crystallite size of 28 nm (that is, powders milled for 16 h).

Conclusions

In the present study, we observed structural changes in high-energy ball-milled Cr_3C_2–25(Ni20Cr) powders, and evidence for this was seen as broadening of the X-ray diffraction peaks. Further, high energy milling decreased the crystallite size of the powders to around 10 nm, and no further decrease was observed even after longer milling times. Severe plastic deformation introduced in the crystal lattice of the milled Cr_3C_2–25(Ni20Cr) powders increased the microstrain at the atomic level. This microstrain increased to a maximum in powders milled for 16 h ($\varepsilon_{max} = 1, 17$ %) and then decreased in powders milled for longer times. The crystallite size of the powder milled for

16 h was 28 nm, indicating this to be the critical crystallite size. The theoretical explanation for our observation regarding lattice strain increasing to a maximum and then decreasing with further deformation is that upon reaching the critical crystallite size, the dislocation structure becomes unstable, which causes the dislocations to dissociate and migrate to the grain boundaries leaving the interior of the grain almost free of dislocations. Thus, "grain boundary sliding" becomes the prevalent mechanism, which is in good agreement with the results of our experiments. Under these conditions, that is near the critical crystallite size, the physical properties of the material are strongly influenced by the grain boundaries, given that a large amount of the atoms present in the material are at the grain and interface boundaries.

Regarding the energy stored in the crystal lattice, due to severe plastic deformation, the heat release observed in our DSC tests revealed a broad transformation, characteristic of a large exothermic reaction. The enthalpy variation measured in the DSC tests permitted determination of the deformation energy stored in the Cr_3C_2–25(Ni20Cr) powders milled for different times. The maximum enthalpy variation measured in the DSC tests was in powders with crystallite size of around 28 nm, and the energy released was of the order of 3025 mJ. These measurements also enabled calculation of the specific heat variation (ΔC_p) of the milled powders.

References

1. Benjamin JS. Dispersion strengthened superalloys by mechanical alloying. Metall Trans. 1970;1:2943–51.
2. Benjamin JS, Volin TE. The mechanism of mechanical alloying. Metall Trans. 1974;5:1929–34.
3. Gilman PS, Benjamin JS. Mechanical alloying. Annu Rev Mater Sci. 1983;13:279–300.
4. Aikin BJM, Courtney TH. The kinetics of composite particle formation during mechanical alloying. Metall Trans. 1993;24A:647–57.
5. He J, Schoenung JM. Nanostructured coatings. Mater Sci Eng. 2002;A336:274–319.
6. He J, Ice M, Lavernia EJ. Synthesis of nanostructured Cr_3C_2–25(Ni20Cr) coatings. Metall Mater Trans. 2000;31A:555–64.
7. Suryanarayana C, Koch CC. In: Suryanarayana C, editor. Non-equilibrium processing of materials. New York: Pergamon; 1999. p. 313–44.
8. Kear BH, Mccandlish LE. Chemical processing and properties of nanostructured WC-Co materials. Nanostruct Mater. 1993;3:19–30.
9. Cunha CA, Lima NB, Martinelli JR, Bressiani AHA, Padial AGF, Ramanathan LV. Microstructure and mechanical properties of thermal sprayed Cr_3C_2-Ni20Cr coatings. Mater Res. 2008;11(2):137–43.
10. Cunha CA, Padial AGF, Lima NB, Martinelli JR, Correa OV, Ramanathan LV. Effect of high energy milling parameters on nanostructured Cr_3C_2-Ni20Cr powder characteristics. Mater Sci Forum. 2008;591–93:282–8.
11. Padial AGF, Cunha CA, Correa OV, Lima NB, Ramanathan LV. Effect of Cr_3C_2-NiCr powder characteristics on structure and properties of thermal sprayed nanostructured coatings. Mater Sci Forum. 2010;660–661:379–84.
12. Sharafi S, Gomari S. Effects of milling and subsequent consolidation treatment on the microstructural properties and hardness of nanocrystalline chromium carbide powders. Int J Refract Met Hard. 2012;30(1):57–63.
13. Jia K, Fisher TE, Gallois B. Microstructure, hardness and toughness of nanostructured and conventional WC-Co composites. Nanostruct Mater. 1998;10:875–91.
14. Roy M, Pauschitz A, Wernisch J, Franek F. The influence of temperature on the wear of Cr_3C_2–25(Ni20Cr) coating—comparison between nanocrystalline grains and conventional grains. Wear. 2004;257:799–811.
15. McCandlish LE, Kear BH, Kim BK. Processing and properties of nanostructured WC-Co. Nanostruct Mater. 1992;1:119–24.
16. Gleiter H. Nanostructured materials: basic concepts and microstructure. Acta Metall Mater. 2000;48:1–29.
17. Birringer R. Nanocrystalline materials. Mater Sci Eng. 1989;7:33–43.
18. Suryanarayana C. Mechanical alloying and milling. Prog Mater Sci. 2001;46:1–184.
19. Rupp J, Birringer R. Enhanced specific-heat-capacity measurements of nanometer-sized crystalline materials. Phys Rev B. 1987;36:7888–90.
20. Hellstern E, Fecht HJ, Fu Z, Johnson WL. Structural and thermodynamic properties of heavily mechanically deformed Ru and AlRu. J Appl Phys. 1989;65:305–10.
21. Yadav TP, Yadav RM, Singh DP. Mechanical milling: a top down approach for the synthesis of nanomaterials and nanocomposites. Nanosci Technol. 2012;2(3):22–48. doi:10.5923/j.nn.20120203.01.
22. He J, Ice M, Lavernia EJ. Synthesis and characterization of nanostructured Cr_3C_2-NiCr. Nanostruct Mater. 1998;10:1271–83.
23. Benjamin JS. Fundamentals of mechanical alloying. In Shingu PH, editor. Mechanical alloying. Mater Sci Forum. 1992. 88–90, p. 1–18.
24. Benjamin JS, Bomford MJ. Dispersion strengthened aluminum made by mechanical alloying. Metall Mater Trans A. 1977;8:1301–5.
25. Koch CC. The synthesis and structure of nanocrystalline material produced by mechanical attrition: a review. Nanostruct Mater. 1993;2:109–29.
26. Koch CC. Synthesis of nanostructured materials by mechanical milling: problems and opportunities. Nanostruct Mater. 1997;9:13–22.
27. Koch CC, Cavin OB, Mckamey CG, Scarbrough JO. Preparation of ''amorphous'' $Ni_{60}Nb_{40}$ by mechanical alloying. Appl Phys Lett. 1983;43:1017–9.
28. Huang B, Perez RJ, Lavernia EJ. Grain growth of nanocrystalline Fe–Al alloys produced by cryomilling in liquid argon and nitrogen. Mater Sci Eng. 1998;A255:124–32.
29. Witkin DB, Lavernia EJ. Synthesis and mechanical behavior of nanostructured materials via cryomilling. Prog Mater Sci. 2006;51:1–60.
30. Han BQ, Lavernia EJ, Mohamed FA. Mechanical behavior of a cryomilled near-nanostructured Al–Mg–Sc alloy. Metall Mater Trans A. 2005;36A:345–55.
31. Dieter GE. Mechanical metallurgy. New York: McGraw-Hill; 1976. p. 236.
32. Coterril P, Mould PR. Recrystallization and grain growth in metals. New York: Wiley; 1976.
33. Warren BE. X-ray diffraction. London: Addison-Wesley; 1959.
34. Cullity BD. Elements of X-ray diffraction. London: Addison-Wesley; 1967.

35. Klug P, Alexander LE. X-ray diffraction procedures. New York: Wiley; 1974. p. 643.
36. Suryanarayana C. X-ray diffraction: a practical approach. New York: Plenum Press; 1998.
37. Rietveld HM. A profile refinement method for nuclear and magnetic structures. J Appl Crystallogr. 1969;2:65–71.
38. Enzo S, Schiffini L. Profile fitting and analytical functions. In: Snyder RL, Fiala J, Bunge HJ, editors. Defect and microstructure analysis by diffraction. New York: Oxford University Press; 1999.
39. Langford JI. Use of pattern decomposition or simulation to study microstructure: theoretical considerations. In: Snyder RL, Fiala J, Bunge HJ, editors. Defect and microstructure analysis by diffraction, International Union of Crystallography. New York: Oxford University Press; 1999.
40. Balzar D. Voigt function model in diffraction-line broadening analysis. In: Snyder RL, Fiala J, Bunge HJ, editors. Defect and microstructure analysis by diffraction, International Union of Crystallography. New York: Oxford University Press; 1999.
41. Pulmtree A, Pawlus LD. Basic questions in fatigue. In: Fong JT, Fields RJ, editors. ASTM STP 924, vol. 1. Philadelphia: American Society for Testing and Materials; 1988. p. 81–97.
42. Xu W, Song X, Lu N, Huang C. Thermodynamic and experimental study on phase stability in nanocrystalline alloys. Acta Mater. 2010;58:396–407.
43. Tjong SC, Chen H. Nanocrystalline materials and coatings. Mater Sci Eng. 2004;R45:1–88.
44. Wolf D, Yamakov V, Phillpot SR, Mukherjee A, Gleiter H. Deformation of nanocrystalline materials by molecular-dynamics simulations: relationship to experiments. Acta Mater. 2005;53:1–40.
45. Cunha CA. Ph.D. Thesis Development of nanostructured Cr_3C_2–25(Ni20Cr) coatings, IPEN, Univ. São Paulo 2012. http://www.teses.usp.br/teses/disponiveis/85/85134/tde-10122012-084041/pt-br.php.
46. Speyer RF. Thermal analysis of materials. New York: Marcel Dekker; 1994. p. 35–45.